A dynamical transition from localized to uniform scrambling in locally hyperbolic systems

Mathias Steinhuber,[1] Peter Schlagheck,[2] Juan Diego Urbina,[1] and Klaus Richter[1]

[1]*Institut für Theoretische Physik, Universität Regensburg, 93040 Regensburg, Germany*
[2]*CESAM Research Unit, University of Liege, 4000 Liège, Belgium*
(Dated: May 17, 2023)

Fast scrambling of quantum correlations, reflected by the exponential growth of Out-of-Time-Order Correlators (OTOCs) on short pre-Ehrenfest time scales, is commonly considered as a major quantum signature of unstable dynamics in quantum systems with a classical limit. In two recent works, by Hummel et al. [1] and by Xu et al. [2], a significant difference in the scrambling rate of integrable (many-body) systems was observed, depending on the initial state being semiclassically localized around unstable fixed points or fully delocalized (infinite temperature). Specifically, the quantum Lyapunov exponent λ_q quantifying the OTOC growth is given, respectively, by $\lambda_q = 2\lambda_s$ or $\lambda_q = \lambda_s$ in terms of the stability exponent λ_s of the hyperbolic fixed point. Here we show that a wave packet, initially localized around this fixed point, features a distinct *dynamical* transition between these two regions. We present an analytical semiclassical approach providing a physical picture of this phenomenon and support our findings by extensive numerical simulations in the whole parameter range of locally unstable dynamics of a Bose-Hubbard dimer. Our results suggest that the existence of this transition is a hallmark of unstable separatrix dynamics in integrable systems. This allows one to distinguish, within the exponential OTOC growth behavior, unstable integrable (many-body) dynamics from genuine chaotic dynamics featuring uniform growth.

I. INTRODUCTION

The scrambling of quantum correlations is an ubiquitous phenomenon across the physics of interacting many-body systems [3, 4]. Its connection to quantum chaos has been established in systems ranging from models for black holes [5–8] to realistic many-body systems such as the SYK-model [9], even comprising systems without a classical limit [10]. Due to the appealing connection with the powerful concepts of quantum chaos, Out-of-Time-Ordered Correlators (OTOCs) [11] represent a major probe of scrambling and thus have received a swiftly increasing huge theoretical interest [3, 5] that has driven efforts for experimental proposals [12] and realizations [13, 14].

In systems with a semiclassical regime, fast scrambling is considered an unambiguous indicator of classical (mean-field) instabilities [4]. As such, Bose-Hubbard systems, with their well understood and controlled classical (mean-field) limit and a large semiclassical region of state space, are prime models to study imprints of scrambling [15–18]. Recently it was shown [1, 19] that an initial exponential growth of OTOCs does not necessarily imply chaotic dynamics of the system's classical counterpart, *i.e.* such OTOC behavior alone cannot serve as clear-cut probe of quantum chaos. These works [1, 19] and further ones picking up the same idea [2, 20–22] show that for quantum (many-body) systems with a classical limit and a semiclassical regime it is sufficient to have local instabilities in a (possibly integrable) phase space to generate exponentially growing OTOCs. Several examples of this situation have been numerical studied [23, 24], including basic models such as an inverted harmonic oscillator [25].

Generically, the prime example of the mechanism for an exponential OTOC growth in an integrable system is the existence of an unstable (hyperbolic) fixed point. Although, by definition, all Lyapunov exponents λ_L are zero in integrable systems, the classical dynamics around fixed points is locally hyperbolic if they have at least one positive stability exponent $\lambda_s > 0$. This type of instability will be considered here. In the early time regime, defined up to a time scale depending logarithmically on the effective Planck constant $\hbar_{eff}$, the OTOCs involving dynamics around unstable points of many-body integrable systems display two markedly different behaviors. In Refs. [1] and [2], the quantum Lyapunov exponents λ_q quantifying the OTOC growth rate are compared to the stability exponents of dominant unstable fixed points of the corresponding classical mean-field dynamics yielding good agreement with $2\lambda_s$ [1] or λ_s [2], respectively.

In this paper we resolve this apparent discrepancy with regard to the operator growth and provide a unified dynamical mechanism explaining the two results in a comprehensive way. We demonstrate that there is a universal $2\lambda_s$ to λ_s transition for the OTOC growth rate λ_q for dynamics around unstable fixed points in the pre-Ehrenfest time regime which interpolates between these two limits. Furthermore, the crossover develops a kink in the strictly classical limit $\hbar_{eff} \to 0$. Moreover, we show that this $2\lambda_s$ to λ_s transition is related to an underlying dynamical transition of the initial quantum state in a phase-space representation and argue that the $2\lambda_s$ to λ_s transition is a hallmark of integrable systems. We propose that this effect can thus be used to distinguish chaotic and integrable systems by properly analyzing the growth behavior of OTOCs at pre-Ehrenfest time scales.

The paper is structured into three further sections. In Sec. II, we present a heuristic argument for OTOCs to exhibit different exponential regimes and the corresponding $2\lambda_s$ to λ_s transition. In order to verify the picture

put forward, we perform an extensive study of the Bose-Hubbard dimer in Sec. III. There, we start with the definition of the dimer and a study of the classical mean-field system including an analytical study of the classical OTOC. Then, numerical results for the OTOCs follow obtained from extensive simulations that display excellent agreement with the classical results for the OTOCs. Furthermore, we show how one can tune the $2\lambda_{\rm s}$ to $\lambda_{\rm s}$-transition, and study its robustness with regard to changing the system parameters. In Sec. IV we summarize our findings and discuss their possible extension to non-integrable systems.

II. OUT-OF-TIME-ORDER CORRELATOR IN INTEGRABLE SYSTEMS WITH LOCAL HYPERBOLICITY

Our goal in this section is to refine the pre-Ehrenfest theory for scrambling around hyperbolic fixed points in integrable systems. In particular we attempt to relax the localization properties of the initial state considered in [1, 2]. The OTOC for two operators $\hat{A}$, $\hat{B}$ with respect to a state $\hat{\rho}$ is defined by

$$\mathbf{C}(t) = {\rm tr}\left\{\hat{\rho}\big|[\hat{A}(t), \hat{B}]\big|^2\right\}, \qquad (1)$$

which is by itself a modulus-squared commutator. When this squared commutator is expanded in individual correlators one obtains, besides contributions that admit a standard time ordering, extra irreducibly un-ordered correlations [5], with anomalous dynamical behavior that are the central object of study.

The long-time (post-Ehrenfest) saturation of generic OTOCs has been subject of several studies, both in the chaotic [18, 26] and integrable [1, 27] regimes where interference effects beyond a pure quasiclassical (Truncated-Wigner like-) approach appear [28].

Here, however, our focus is the short time scales, where a quasiclassical approach based on the Wigner-Moyal expansion, which is a regular expansion around $\hbar_{\rm eff} = 0$ [29–31], is perfectly appropriate. Keeping only leading-order terms in $\hbar_{\rm eff}$, one obtains

$$\mathbf{C}(t) = \hbar_{\rm eff}{}^2 \langle W_\rho(\vec{q}_0, \vec{p}_0) \big| \left\{A_{\rm W}(\vec{q}_0, \vec{p}_0, t), B_{\rm W}(\vec{q}_0, \vec{p}_0)\right\}\big|^2 \rangle_{\rm PS} \\ + O(\hbar_{\rm eff}{}^3), \qquad (2)$$

where A_W, B_W are the Wigner-transforms of the operators $\hat{A}$, $\hat{B}$ and $W_\rho(\vec{q}_0, \vec{p}_0)$ is the Wigner-distribution corresponding to the state $\hat{\rho}$. A detailed derivation of Eq. (2) is in App. V A.

Further, $\langle . \rangle_{\rm PS}$ indicates integration over the whole classical (mean-field) phase space parametrized by the canonical pairs $(\vec{q}_0, \vec{p}_0)$. The Heisenberg time dynamics of the quantum operator is mapped to time dynamics of the classical observable $A(q_0, p_0, t) =$ dynamics of the classical observable $A(q_0, p_0, t) =$

$A(q(q_0, p_0, t), p(q_0, p_0, t))$ which arises from the classical propagation of the initial condition (q_0, p_0).

The effective Plank constant $\hbar_{\rm eff}$ has different expressions in different contexts. It is given by the usual Plank constant divided a typical action $\hbar/S_{\rm typ}$ in single particle cases [32–34], and the inverse of the total spin quantum number $1/S$ for spin systems [35, 36]. In the case of interest here, interacting bosonic systems, $\hbar_{\rm eff} = \frac{1}{N}$ is given by the inverse of the total particle number N after convenient rescaling of the interaction strength [4, 37].

Without loss of generality, we choose the operators $\hat{A} = \hat{q}$ and $\hat{B} = \hat{p}$, as they are hermitian and their classical counterparts are generalized coordinates or momenta. Therefore, at leading order in the Wigner-Moyal expansion, Eq. (2), we drop the index $_W$ and take the pure classical phase space functions. This choice of the operators simplifies the classical Poisson-brackets, that are now given by an element of the stability matrix $\frac{\partial \vec{x}(t)}{\partial \vec{x}(0)}$ with $\vec{x} = (\vec{q}, \vec{p})$ [38, 39].

The classical limit of the OTOC in Eq. (2) is so far a completely general result. Under the assumption of local instability, however, the leading order of exponential growth is given by the maximal local exponent $\lambda(\vec{q}_0, \vec{p}_0)$ of the stability matrix:

$$\mathbf{C}(t) \sim \hbar_{\rm eff}{}^2 \langle W_\rho(\vec{q}_0, \vec{p}_0) \exp\left\{2\lambda(\vec{q}_0, \vec{p}_0)t\right\}\rangle_{\rm PS}. \qquad (3)$$

At this point, it is convenient to introduce two local time-scales:

- After the local ergodic time $\tau_{\rm s} = 1/\lambda(\vec{q}_0, \vec{p}_0)$, the exponential growth of the OTOC begins to be visible. Before $\tau_{\rm s}$, we have sub-exponential/polynomial behavior linked to system-specific mechanisms.

- The Wigner-Weyl approximation breaks down when the leading order of the integrand in Eq. (2) becomes large compared to $\hbar_{\rm eff}{}^2$. This breakdown defines the local Ehrenfest time $\tau_{\rm E} = \lambda^{-1}(\vec{q}_0, \vec{p}_0) \log(1/\hbar_{\rm eff})$ and in our many-body case $\tau_{\rm E} = \lambda^{-1}(\vec{q}_0, \vec{p}_0) \log N$.

We exploit the experimentally tunable localization features of quantum mechanical states [40] as a tool to probe the local unstable dynamics around a hyperbolic fixed point (FP) and consider a coherent-like state $\hat{\rho}$ centered around it. In the linearized region around the FP the dynamics can be precisely described, and we can express $\lambda(\vec{q}_0, \vec{p}_0)$ by the maximal stability exponent $\lambda_{\rm s}$ of the FP. In general, however, the linearized region is bounded and we express this by the fact that the relation $\{A(\vec{q}_0, \vec{p}_0, t), B(\vec{q}_0, \vec{p}_0)\} = e^{\lambda_{\rm s} t}$ is valid only if the unstable manifold coordinate/projection $u(\vec{q}_0, \vec{p}_0)$ is smaller than a threshold $c > 0$. For times larger than zero, the exponential growth $u(\vec{q}_0, \vec{p}_0, t) = u(\vec{q}_0, \vec{p}_0)e^{\lambda_{\rm s} t}$ is only valid if the linearized region $u(\vec{q}(t), \vec{p}(t), t) < c$ is still fulfilled. Afterwards we need to replace the time dynamics of the unstable manifold by a sub-exponential function. We refer to this mechanism as a kind of *leaking* from the linearized region [2].

The key observation is that, although the sub-exponential function describes the classical evolution outside and it is therefore negligibly small compared to the exponential growth in the linearized region, its contribution is weighted by a portion of phase space that grows exponentially. These considerations allow us to heuristically account for the leaking mechanism, by modifying the Eq. (3) as

$$\mathbf{C}(t) \sim \hbar_{\mathrm{eff}}{}^2 e^{2\lambda_{\mathrm{s}} t} \langle W_\rho(\vec{q}_0, \vec{p}_0) \Theta(c - e^{\lambda_{\mathrm{s}} t} u(\vec{q}_0, \vec{p}_0)) \rangle_{\mathrm{LR}}, \tag{4}$$

where we restrict the phase-space integration to the dominant linearized region (LR) around the FP.

For definiteness, let us consider now a Gaussian wave-packet with an initial linear width Δu along the unstable manifold $u(\vec{q}, \vec{p})$. In this situation, the wave-packet reaches the boundary of the linear region by a finite time $\tau_{\mathrm{L}} = \lambda_{\mathrm{s}}^{-1} \ln(c/\Delta u)$, which we correspondingly call the leaking time. After τ_{L}, we must take the leaking of the wave-packet into account, i.e., the phase-space volume causing the exponential growth shrinks exponentially with $e^{-\lambda_{\mathrm{s}} t}$, i.e.,

$$\langle W_\rho(\vec{q}_0, \vec{p}_0) \Theta(c - e^{\lambda_{\mathrm{s}} t} u(\vec{q}_0, \vec{p}_0)) \rangle_{\mathrm{LR}} \sim \begin{cases} \mathrm{const.} & , t < \tau_{\mathrm{L}} \\ e^{-\lambda_{\mathrm{s}} t} & , t > \tau_{\mathrm{L}} \end{cases}.$$

Hence, the exponential growth of the OTOC in Eq. (4) decreases to $e^{\lambda_{\mathrm{s}} t}$. This finally leads to a short-time behavior of the OTOC around an unstable fixed point given by

$$\mathbf{C}(t) \sim \begin{cases} \mathrm{poly.} & , t < \tau_{\mathrm{s}} \\ e^{2\lambda_{\mathrm{s}} t} & , \tau_{\mathrm{s}} < t < \tau_{\mathrm{L}} \\ e^{\lambda_{\mathrm{s}} t} & , \tau_{\mathrm{L}} < t < \tau_{\mathrm{E}} \\ \mathrm{osc.} & , \tau_{\mathrm{E}} < t \end{cases}, \tag{5}$$

that is schematically displayed in Fig. 1 showing two exponential regions.

It is important to note that there is a hierarchy of time scales: the leaking time is only relevant if $\tau_{\mathrm{L}} < \tau_{\mathrm{E}}$, otherwise the Wigner-Weyl approximation (in leading order), see Eq. (2), is already invalid.

The initial linear width Δu scales with some power $\hbar_{\mathrm{eff}}^\alpha$ for typical states. This gives an asymptotic expression for the leaking time by $\tau_{\mathrm{L}} \sim \frac{\alpha}{\lambda_{\mathrm{s}}} \log N + O(\log(c))$. Hence, we have a direct proportional relation to the Ehrenfest time $\tau_{\mathrm{L}} \sim \alpha \tau_{\mathrm{E}}$ for $\hbar_{\mathrm{eff}} \to 0$.

We see then, that one can clearly distinguish three parametric regions: $\tau_{\mathrm{L}} < \tau_{\mathrm{s}}$, $\tau_{\mathrm{s}} < \tau_{\mathrm{L}} < \tau_{\mathrm{E}}$ and $\tau_{\mathrm{E}} \leq \tau_{\mathrm{L}}$ (which is equivalent to $\alpha \approx 0, < 1, \approx 1$):

i) Delocalized/uniform states: $\tau_{\mathrm{L}} < \tau_{\mathrm{s}}$, $\alpha \approx 0$
   Under the assumption that there is only one unstable FP of the classical dynamics, the OTOC is still governed by Eq. (5) and the $e^{2\lambda_{\mathrm{s}} t}$-regime vanishes. A typical examples here are high temperature states ($T \to \infty$).

ii) Localized states: $\tau_{\mathrm{s}} < \tau_{\mathrm{L}} < \tau_{\mathrm{E}}$, $0 < \alpha < 1$
   In this case we have the $2\lambda_{\mathrm{s}} - \lambda_{\mathrm{s}}$ transition and
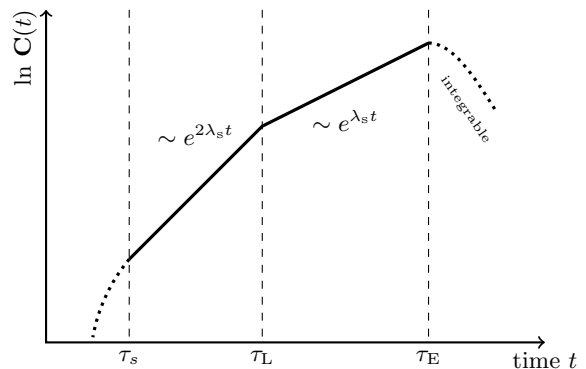
FIG. 1. Expected behavior of an OTOC centered at a FP if $\tau_{\mathrm{s}} < \tau_{\mathrm{L}} < \tau_{\mathrm{E}}$: OTOCs grow polynomial for times shorter τ_{s}, exponential with $2\lambda_{\mathrm{s}}$ for times shorter τ_{L}, exponential with λ_{s} for times shorter τ_{E}, but greater than τ_{L}. Post-Ehrenfest time scales display oscillatory behaviour if the system is integrable [27] and saturation if the system is chaotic [18, 41].

asymptotically (for $N \to \infty$) we expect a sharp kink to appear at τ_{L}. The prime example are the coherent states centered at a FP. They usually have a linear size of $\hbar_{\mathrm{eff}}^{1/2}$ in all phase space directions.

iii) Well-localized states: $\tau_{\mathrm{L}} \approx \tau_{\mathrm{E}}$, $\alpha \approx 1$
   The second $e^{\lambda_{\mathrm{s}} t}$-region is vanishing, only the one $e^{2\lambda_{\mathrm{s}} t}$-region is visible. Fock states are candidates for the third class. Their linear width is $\hbar_{\mathrm{eff}}$ in the classical occupation numbers, such that $\alpha \approx 1$ if the unstable manifold is aligned in the parallel direction.

The case $\alpha > 1$ is unphysical and can be excluded. The uncertainty principle requires the product of the width in all directions to be $\geq \hbar_{\mathrm{eff}}/2$. Hence if $\alpha > 1$, one direction must increase if $\hbar_{\mathrm{eff}} \to 0$, i.e., this direction becomes delocalized if we approach the classical limit contradicting that the state is associated by a well-defined point in phase space.

At this point, we can explain the dynamical behavior of OTOCs reported in [1] and [2]. In the first paper, the authors investigated a number-projected coherent state which is simultaneously a Fock state. Its unstable manifold is parallel to the occupation direction [42], therefore it falls into the case iii) and they see only the $2\lambda_{\mathrm{s}}$-exponential window. Correspondingly, the authors of the second paper use the infinite temperature state, hence their state directly falls into the first case and the only exponential window is given by $e^{\lambda_{\mathrm{s}} t}$.

In the next section, we numerically explore the validity Eq. (5) for a Bose-Hubbard dimer, with the aim of carefully investigate the new case ii), where the hierarchy of time scales $\tau_{\mathrm{s}} < \tau_{\mathrm{L}} < \tau_{\mathrm{E}}$ implies, from our analysis, the presence of a $2\lambda_{\mathrm{s}} - \lambda_{\mathrm{s}}$ transition.

III. BOSE-HUBBARD DIMER

The Bose-Hubbard dimer describes bosonic degrees of freedom occupying two discrete levels or sites. Prime physical setups are individual Josephson-junctions [43] or cold atoms within a small two-sited optical lattice [44–49]. In all these cases, one ends with an effective description in terms of the following Hamiltonian

$$\hat{H} = -2J\big(\hat{a}_2^\dagger \hat{a}_1 + \hat{a}_2 \hat{a}_1^\dagger\big) + \frac{g}{2}\big(\hat{a}_1^{\dagger 2}\hat{a}_1^2 + \hat{a}_2^{\dagger 2}\hat{a}_2^2\big), \quad (6)$$

where the parameter J is the hopping and g is the (local) interaction strength between particles given in units of energy. Our Hamiltonian differs from the usual dimer Hamiltonian, the hopping coefficient $2J$ (instead of J) is motivated to be consistent with a ring topology for higher number of wells. Consequently, the two-site ring has a doubly counted hopping term. We also introduce a new dimensionless parameter Θ such that we have $J = \epsilon_0 \cos \Theta$ and $g = \epsilon_0 \frac{2}{N} \sin \Theta$, with $\epsilon_0 = \sqrt{J^2 + (gN/2)^2}$ representing a global energy scale. We set $\epsilon_0 = 1$ for a convenient unit system, yielding also the time unit $\hbar/\epsilon_0 = 1$. The parameter space is thus compactified to $\Theta \in [-\pi/2, \pi/2]$.

A. Classical mean-field limit

We follow the standard approach [50] to derive the classical limit for bosons and replace the operators by complex numbers

$$\hat{a}_j, \hat{a}_j^\dagger \;\longmapsto\; \psi_j, \psi_j^*$$

within the normal-ordered quantum Hamiltonian in Eq. (6) to obtain a classical mean-field system. The discrete nonlinear Schrödinger equation $i\dot{\psi}_j = \frac{\partial H}{\partial \psi_j^*}$ yields Hamilton's equations of motion that define the classical dynamics. Due to the conserved total particle number N, we define new set of conjugated classical variables

$$N = n_1 + n_2, \quad \phi = \tfrac{1}{2}(\varphi_1 + \varphi_2),$$
$$n = \tfrac{1}{2}(n_1 - n_2), \quad \varphi = \varphi_1 - \varphi_2 - \pi,$$

where the two mean fields $\psi_j = \sqrt{n_j}e^{i\varphi_j}$ are written in phase φ_j and occupations n_j. Hence, the Hamiltonian takes the form

$$H(N, \phi, n, \varphi) = 2\cos\Theta \sqrt{N^2 - 4n^2} \cos\varphi$$
$$+ \sin\Theta \Big(\frac{2n^2}{N} + \frac{N}{2}\Big). \quad (7)$$

We can reduce the dynamics to a one-dimensional system with a single conjugated pair ($z = 2n/N$, $\varphi = \varphi_1 - \varphi_2 - \pi$) given by the population inversion and relative phase [51]. With these coordinates, we can reduce the equations of motion to two coupled real-valued ODEs

$$\dot{z} = -4\cos\Theta \sqrt{1 - z^2} \sin\varphi,$$
$$\dot{\varphi} = 4\cos\Theta \frac{z\cos\varphi}{\sqrt{1 - z^2}} - 2\sin\Theta\, z, \quad (8)$$
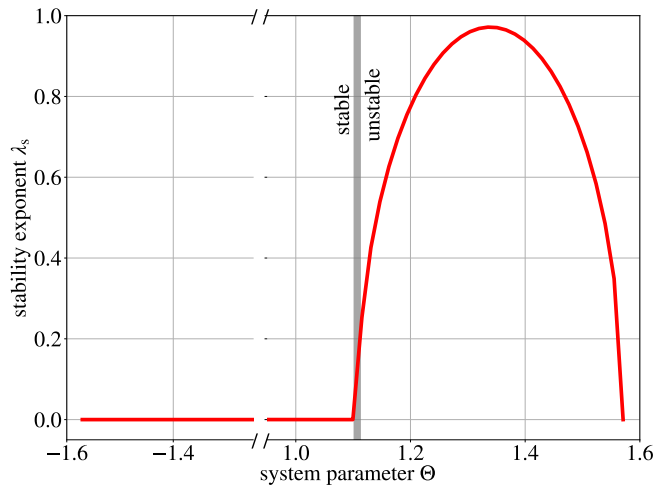

FIG. 2. Stability exponent of the off-phase FP over the whole parameter space. A change from stable to unstable behaviour occurs at the bifurcation point $\Theta = \arctan 2$.

which is a one-degree-of-freedom system. Conveniently, the mean-field system deriving from Eq. (8) is integrable and can thus be exactly solved up to quadrature.

B. Fixed points

A straightforward calculation shows that there are two fixed points (FPs), at ($z = 0$, $\varphi = \pi$) and ($z = 0$, $\varphi = 0$), which are independent of the system parameter Θ. We call these two FPs the *in-phase* and *off-phase* FP, since both have homogeneous occupations and a zero or π phase difference between site 1 and 2. We set the zero point for the relative phase φ to the unstable off-phase FP.

Two bifurcations appear: at $\Theta = -\arctan 2$ for the in-phase FP and at $\Theta = \arctan 2$ for off-phase FP. We restrict our discussion to the off-phase FP, since there is a symmetry between these two PFs under a change of sign of the parameter Θ. The stability diagram of the off-phase FP, displayed in Fig. 2, shows the bifurcation at $\arctan 2$, where the stability exponent becomes positive. Its maximum $\lambda_s = 0.97$ is reached at $\Theta_* \approx 1.35$.

Fig. 3 shows the reduced phase space structure of the system, generated by Eq. (8), at the maximal unstable parameter Θ_*. Note in particular the (red) separatrix defined by the unstable and stable manifold originating from the off-phase FP. The merging of stable and unstable manifolds indicates that the linearized regime is bounded, namely, any classical trajectory on the unstable manifolds converges to the stable manifold leading (in infinite time) back to the hyperbolic FP. The exact size of the linearized regime, modeled by the constant c in the previous Sec. II, plays a negligible role for $\hbar_{\text{eff}} \to 0$, since it is additive and $\hbar_{\text{eff}}$-independent constant in the leaking time $\tau_L = \lambda_s^{-1} \ln(c/\Delta u) \sim \lambda_s^{-1} \ln(1/\hbar_{\text{eff}}))/2 + \lambda_s^{-1} \ln c$ in

Eq. (4) with $\Delta u \sim \hbar_{\text{eff}}^{1/2}$ (for a coherent state). Therefore we leave c unspecified in the subsequent discussion.
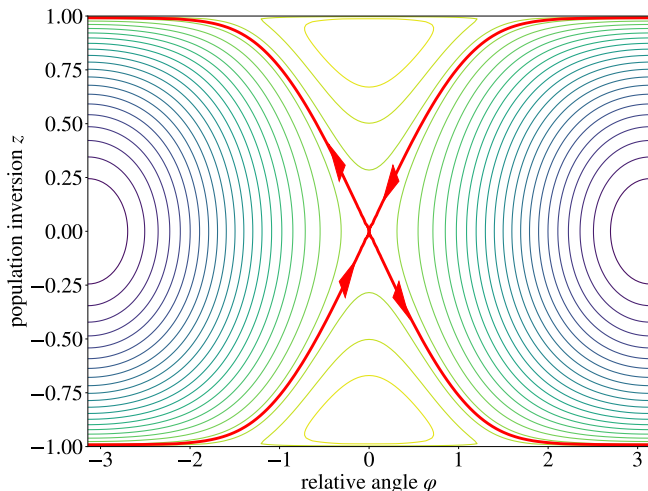

FIG. 3. Reduced phase space structure (z, φ) for Θ_*: contour lines of the Hamiltonian correspond to the classical trajectories. There are three elliptic fixed points and one hyperbolic fixed point whose associated separatrix is highlighted in red. Arrows on the separatrix indicate the stable and unstable manifolds.

Armed with this very specific phase-space structure, we carry an in-depth analytical study of the OTOC $\mathbf{C}(t)$ for the dimer in the next section.

C. Microscopic approach: separatrix dynamics

We choose for the dimer the operators $\hat{A} = \hat{B} = \hat{n}_1$ to be the number operator $\hat{n}_1 = \hat{a}_1^\dagger \hat{a}_1$ at the first site. Therefore, we get

$$\mathbf{C}(t) = \langle ||[\hat{n}_1(t), \hat{n}_1]||^2 \rangle = \langle ||[\hat{n}(t), \hat{n}]||^2 \rangle , \quad (9)$$

where $\hat{n} = \frac{1}{2}(\hat{n}_1 - \hat{n}_2)$. For this OTOC, we are interested in evaluating the classical expression which is given by

$$O(t) = \iint dn \, d\varphi \, W(n, \varphi) \left(\frac{\partial n_t}{\partial \varphi_0} \right)^2 , \quad (10)$$

with $W(n, \varphi)$ the Wigner function associated with the initial state. The latter is, for the sake of simplicity, modeled as a coherent quantum state $\exp\left(\sqrt{N_0}(\hat{a}_-^\dagger - \hat{a}_-)\right)|0\rangle$ with $\hat{a}_- = \hat{a}_1 - \hat{a}_2$, keeping in mind that for large N_0 this coherent state features very similar properties as a number-projected coherent state with total particle number N_0 as far as the site population exchange dynamics is concerned. The Wigner function associated with this initial state would be given

by

$$W(N, \phi, n, \varphi) \simeq$$
$$\frac{1}{\pi^2} \exp\left(-\frac{(N - N_0)^2}{2N_0} - 2N_0\phi^2 - \frac{2n^2}{N_0} - \frac{N_0\varphi^2}{2}\right) \quad (11)$$

in the framework of a quadratic expansion valid for $N_0 \gg 1$. Since the Wigner function W describes a tight localization of N about N_0, we set $N_0 = N$ henceforth and model the initial quantum state concerning the intersite population exchange dynamics by the Wigner function

$$W(n, \varphi) = \frac{1}{\pi} \exp\left(-\frac{2n^2}{\omega N} - \frac{N\omega\varphi^2}{2}\right) , \quad (12)$$

where the squeezing parameter ω allows for some flexibility in the definition of the initial quantum state.

Let us first discuss the linearized dynamics in the near vicinity of the FP $(n, \varphi) = (0, 0)$. Linearizing Eq. (8), we obtain the system of equations

$$\dot{z} = -4\cos\Theta\varphi ,$$
$$\dot{\varphi} = -2(\sin\Theta - 2\cos\Theta)z , \quad (13)$$

which is readily solved as

$$z_t = z_0 \cosh\lambda_s t - \frac{4\cos\Theta\varphi_0}{\lambda_s} \sinh\lambda_s t ,$$
$$\varphi_t = \varphi_0 \cosh\lambda_s t - \frac{\lambda_s z_0}{4\cos\Theta} \sinh\lambda_s t \quad (14)$$

in terms of the stability exponent

$$\lambda_s = 4\cos\Theta\sqrt{\frac{\gamma}{2} - 1} , \quad (15)$$

where we defined the nonlinearity parameter $\gamma = \tan\Theta = gN/(LJ)$. The latter becomes purely imaginary for $\gamma < 2$, which implies that $(n, \varphi) = (0, 0)$ turns into a stable fixed point if the nonlinearity parameter γ is decreased below two, as it is plotted in Fig. 2.

Considering $\gamma > 2$ henceforth, and assuming that the point (z_0, φ_0) is located very closely to the origin in this phase space, we can, as in the previous section, identify a time scale $\tau_s \gg \lambda_s^{-1}$ for which we still have $|z_{\tau_s}| \ll 1$ and $|\varphi_{\tau_s}| \ll 1$, such that the above linearization Eq. (13) of the classical equations of motion remains valid until $t = \tau_s$. Since at the same time we have $\lambda_s \tau_s \gg 1$ by assumption, the solution Eq. (14) of the linearized equation Eq. (13) for $t = \tau_s$ simplifies as

$$z_{\tau_s} = \left(\frac{z_0}{2} - \frac{2\cos\Theta\varphi_0}{\lambda_s}\right) e^{\lambda_s\tau_s} , \quad (16)$$

$$\varphi_{\tau_s} = \left(\frac{\varphi_0}{2} - \frac{\lambda_s z_0}{8\cos\Theta}\right) e^{\lambda_s\tau_s} . \quad (17)$$

From the time τ_s on, we can safely assume that the trajectory under consideration very closely follows the separatrix structure emanating from the unstable antihom.

fixed point $(z, \varphi) = (0, 0)$. This separatrix structure is obtained through the identification of the energy

$$H(n, \varphi) = 2 \cos \Theta N + \sin \Theta \frac{N}{2} \qquad (18)$$

of the classical Hamiltonian Eq. (7), from which follows the identity

$$\cos \varphi = \frac{1 - \frac{\gamma}{4} z^2}{\sqrt{1 - z^2}}.$$

Inserting this expression into Eq. (8) yields the differential equation

$$\dot{z} = z \sqrt{\lambda_s^2 - \sin^2 \Theta z^2}$$

describing the motion along the upper or lower separatrix branch. This equation is straightforwardly integrated yielding

$$t - \tau_s = \int_{z_{\tau_s}}^{z_t} \frac{dz}{z \sqrt{\lambda_s^2 - \sin^2 \Theta z^2}}$$

$$= -\frac{1}{\lambda_s} \left[\operatorname{arcosh} \left(\frac{\lambda_s}{\sin \Theta |z_t|} \right) - \operatorname{arcosh} \left(\frac{\lambda_s}{\sin \Theta |z_{\tau_s}|} \right) \right],$$

from which we obtain

$$z_t = \frac{\operatorname{sgn}(z_{\tau_s}) \lambda_s / \sin \Theta}{\cosh \left[\operatorname{arcosh} \left(\frac{\lambda_s}{\sin \Theta |z_{\tau_s}|} \right) - \lambda_s (t - \tau_s) \right]}. \qquad (19)$$

Using $|z_{\tau_s}| \ll 1$ and hence also $\sin \Theta |z_{\tau_s}| / \lambda_s \ll 1$ for finite values of $\sin \Theta$ and λ_s, we define

$$x_t = \operatorname{sgn}(z_{\tau_s}) \exp \left[-\operatorname{arcosh} \left(\frac{\lambda_s}{\gamma |z_{\tau_s}|} \right) + \lambda_s (t - \tau_s) \right]$$

$$\simeq \frac{\sin \Theta}{2 \lambda_s} \left(\frac{z_0}{2} - 2 \cos \Theta \frac{\varphi_0}{\lambda_s} \right) e^{\lambda_s t} \qquad (20)$$

$$\simeq \frac{\sin \Theta}{\lambda_s} \left(\frac{n_0}{N} - 2 \cos \Theta \frac{\varphi_0}{\lambda_s} \right) \sinh(\lambda_s t),$$

where we make use of the asymptotic expression

$$\operatorname{arcosh}(u) = \ln \left(u + \sqrt{u^2 - 1} \right) \simeq \ln(2u) + O(u^{-2}) \quad (21)$$

for large u, in combination with Eq. (16). With $(\cosh u)^{-1} = 2 e^u / (1 + e^{2u})$ we can thus rewrite Eq. (19) in terms of the expression Eq. (20) as

$$z_\tau = \frac{2 \lambda_s}{\sin \Theta} \frac{x_t}{1 + x_t^2}, \qquad (22)$$

which yields

$$n_t = \frac{N \lambda_s}{\sin \Theta} \frac{x_t}{1 + x_t^2}. \qquad (23)$$

Replacing $e^{\lambda_s t}$ with $2 \sinh(\lambda_s t)$ in Eq. (20) is clearly valid for large $\lambda_s t \gg 1$ and has the additional advantage that

the short-time regime in the time evolution of n_t will thereby be correctly captured as well within Eq. (23).

The classical limit of the quantum OTOC, Eq. (10), is then evaluated as

$$O(t) = \frac{2 \cos^2 \Theta N^2}{\sqrt{\pi} a \lambda_s^2} \sinh(\lambda_s t)$$

$$\int \frac{(1 - x^2)^2}{(1 + x^2)^4} \exp \left[-\left(\frac{x}{2a \sinh(\lambda_s t)} \right)^2 \right] dx \qquad (24)$$

where the dimensionless scale is defined as

$$a = \frac{\sin \Theta / \lambda_s}{\sqrt{8 \omega N}} \sqrt{\omega^2 + \frac{16 \cos^2 \Theta}{\lambda_s^2}}. \qquad (25)$$

The short-time behavior of the OTOC, for $t \ll \tau_L = -\lambda_s^{-1} \ln a$, is yielded as

$$O(t) \simeq 4 \cos^2 \Theta \frac{N^2}{\lambda_s^2} \sinh^2(\lambda_s t), \qquad (26)$$

while for $t \gg \tau_L$ we obtain

$$O(t) \simeq \cos^2 \Theta \frac{\sqrt{\pi} N^2}{4a \lambda_s^2} e^{\lambda_s t}. \qquad (27)$$

These two limits correspond to the $2 \lambda_s - \lambda_s$ transition that we heuristically derived in Sec. II, as expressed in Eq. (5). Note that the here defined τ_L agrees with the case ii) in Sec. II. The dimensionless constant $\ln a$ encodes the linear width of the wave-packet along the unstable direction.

With this detailed classical calculation at hand, we analyze the OTOC centered around this local hyperbolic off-phase FP, considering the parameter Θ_* at which the value of the stability exponent is maximal, $\lambda_s = 0.97$.

D. Numerical results for the Out-of-Time-Order Correlator

We proceed now with the numerical study and calculate the OTOC via Eq. (9) by means of numerically exact simulations for the operators $\hat{A} = \hat{B} = \hat{n}_1$. We consider the state

$$|\vec{\xi}\rangle = \frac{1}{\mathcal{N}} \left(\xi_1 \hat{a}_1^\dagger + \xi_2 \hat{a}_2^\dagger \right)^N |0\rangle, \qquad (28)$$

which is a number-projected coherent state centered at the off-phase FP $\vec{\xi} = (\xi_1, \xi_2) = (\sqrt{N/2}, -\sqrt{N/2})$, with $\mathcal{N} = \sqrt{N^N N!}$ a normalization constant.

For large total particle number N, the projected coherent state inherits properties from the coherent state, in particular the linear width of $\hbar_{\text{eff}}^{1/2}$ in each phase space direction [52], including the unstable direction in Fig. 3. Furthermore it sets the squeezing parameter $\omega = 1$ in the classical analysis in Eq. (25). Following the discussion in Sec. II, case ii), the leaking time τ_L is therefore half the
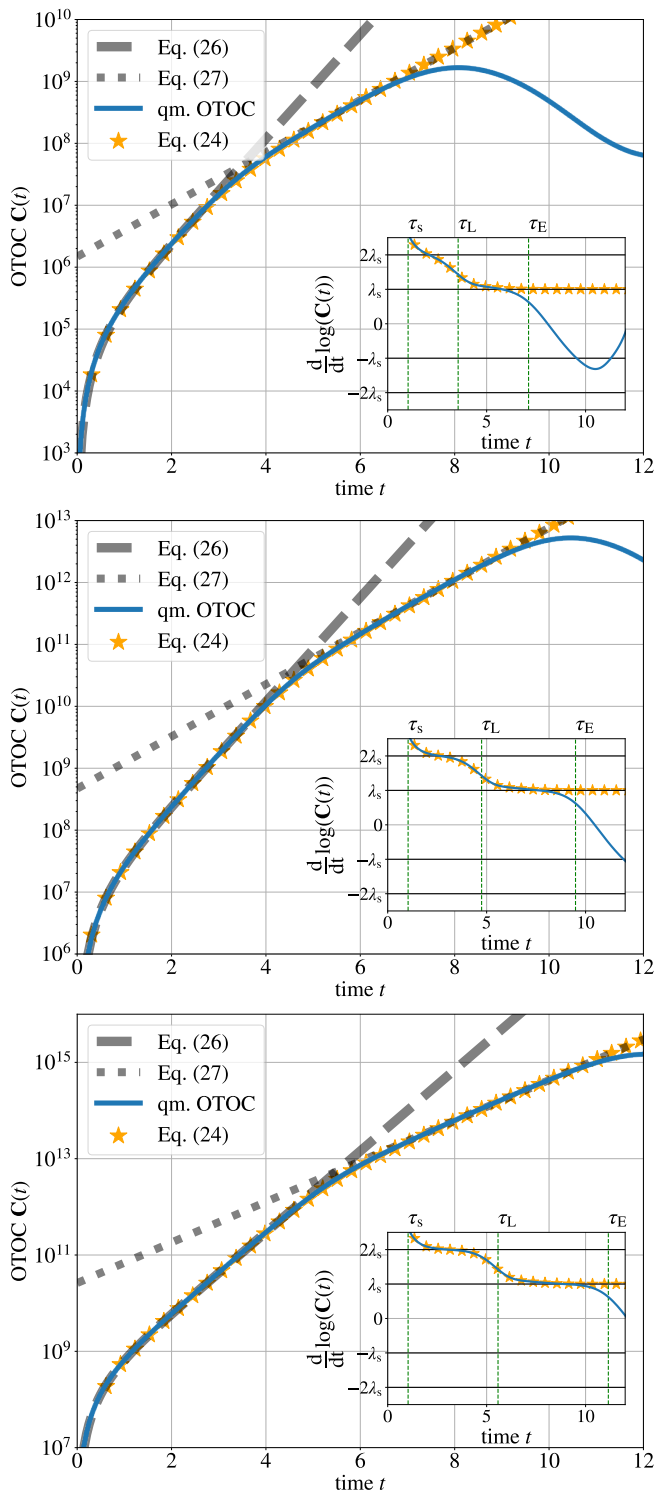
FIG. 4. Top to bottom: OTOC $\mathbf{C}(t)$ for $N = 10^3$, 10^4, $5 \cdot 10^4$ and $\Theta = 1.35$; shaping kink from the $2\lambda_s - \lambda_s$ transition at $\tau_L = \tau_E/2$; the classical expressions Eq. (26) and Eq. (27) fit tightly the OTOC in each region showing $\exp(2\lambda_s t)$ and $\exp(\lambda_s t)$ exponential growth rates.

Ehrenfest time τ_E. We display our numerical OTOCs for increasing particle $N = 10^3$, 10^4, $5 \cdot 10^4$ in Fig. 4,

where we observe the predicted $2\lambda_s - \lambda_s$ transition, precisely following the heuristic arguments of Sec. II and the more refined classical analysis of Sec. III C. In particular, the analytical result Eq. (24) for the classical OTOC follows perfectly the quantum OTOC $\mathbf{C}(t)$, i.e., it captures both regimes and the transition. The kink at the transition becomes sharper for $N \to \infty$. This is also seen in the insets showing the time-derivative of $\log(\mathbf{C}(t))$, which confirm that with increasing N there are more and more pronounced $2\lambda_s$ and λ_s regions of exponential growth.

In order to illustrate the leaking from the linearized region around the FP, we visualize in Fig. 5, via its Husimi distribution, the time evolution of a wave packet that emanates from the coherent state Eq. (28) with $N = 10^3$. With time, the wave packet spreads along the separatrix and evolves to the upper right and lower left corners of the phase space. We see that at the time $\tau_L = \tau_E/2$ the wave packet folds back from the unstable to the stable manifold. This back-folding corresponds to the dynamical transition of leaking from the linearized regime.

Calculations for different values of the system parameter Θ yield qualitatively similar behavior in the range where the off-phase FP is unstable, again with excellent agreement between the quantum OTOC Eq. (9) and its classical approximation Eq. (24). To demonstrate this we compute the relative logarithmic deviation between Eq. (24) and Eq. (9), defined by

$$\eta(t) = \left| \frac{\ln O(t) - \ln \mathbf{C}(t)}{\ln O(t)} \right| \qquad (29)$$

for the number projected state $|\vec{\xi}\rangle$. Fig. 6 displays, for various choices of the total particle number N, the time evolution of η up to the Ehrenfest time for $\Theta = 1.35$ (right panel) as well as its maximal value

$$\eta_{\max} = \max_{t \leq 0.8\tau_E} \eta(t) \qquad (30)$$

in the interval $0 \leq t \leq 0.8\tau_E$ as a function of Θ (left panel). At the edges of the instability region (i.e., for $\Theta \to \arctan(2)$ or $\pi/2$) the maximal deviation significantly increases, since there we have $\lambda_s \to 0$ and thus cannot, for finite $\hbar_{\text{eff}}$, justify the assumption that the time evolution of all phase-space points covered by the initial Wigner function very closely follows the separatrix arc. Nevertheless, the deviations clearly tend to zero in the semiclassical limit $\hbar_{\text{eff}} \to 0$, independently of the values of $\Theta \in (\arctan(2), \pi/2)$ and $t \in [0, \tau_E]$. This confirms that the $2\lambda_s - \lambda_s$ transition is independent of the specific value of Θ, i.e., it is a robust signal of a dynamical transition.

E. Squeezing – engineering the leaking time τ_L

An important consequence of the leaking mechanism is that the linear extent of the initial state along the unstable manifolds is the key ingredient for the exact
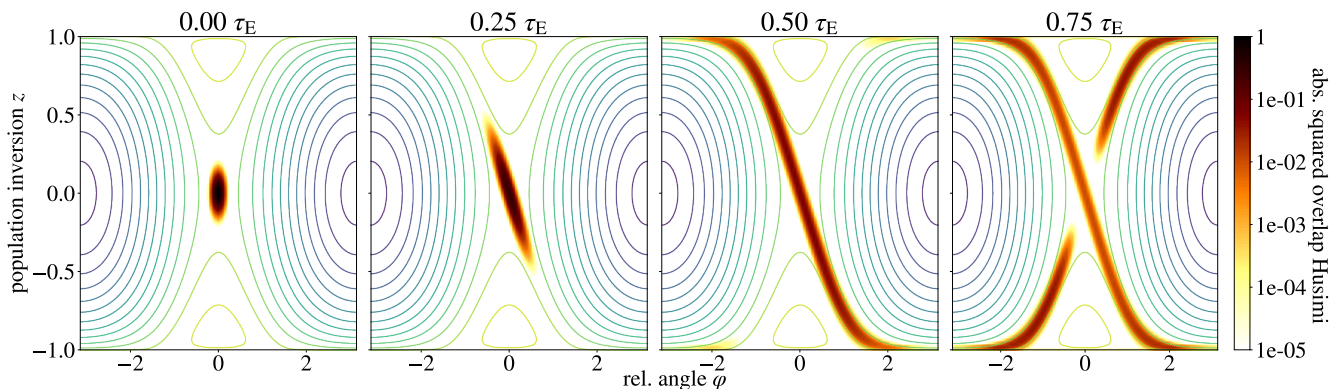
FIG. 5. Time-evolution of the Husimi-distribution for the state $|\vec{\xi}\rangle$ centered at the hyperbolic off-phase FP with $N = 10^3$ particles. We observe scrambling along the unstable manifold on the separatrix until $t \approx \tau_{\mathrm{L}}$.
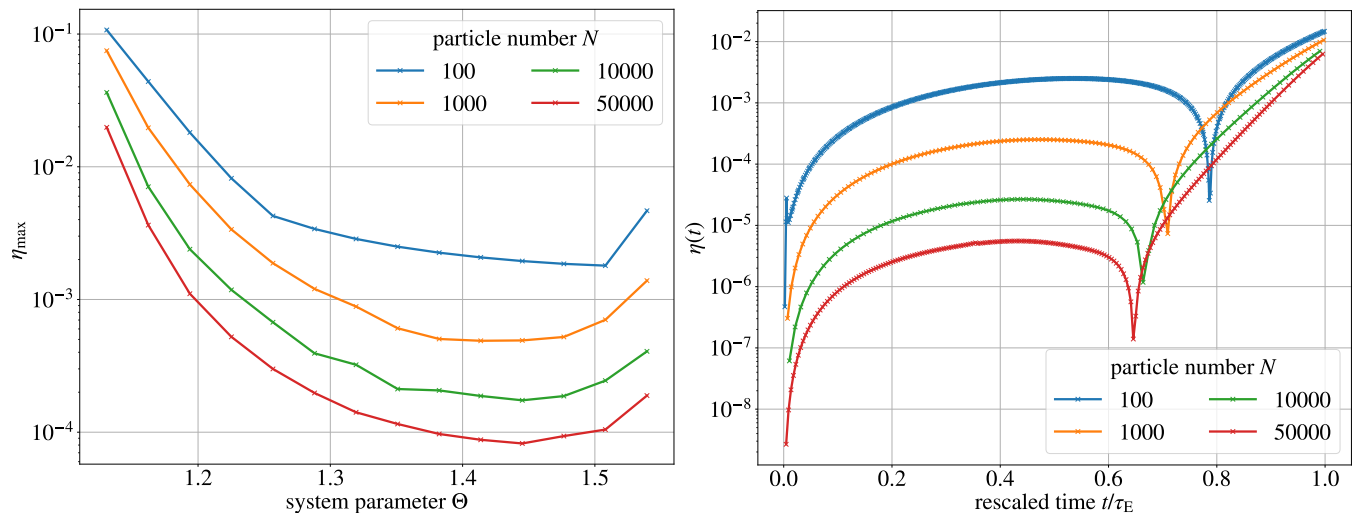

FIG. 6. Left panel: maximal relative logarithmic deviation Eq. (30) plotted as a function of the system parameter Θ in the instability region. Right panel: relative logarithmic deviation Eq. (29) plotted as a function of time for $\Theta = 1.35$. The calculations were done for the total particle numbers (from top to bottom) $N = 100$, 1000, 10000, and 50000.

position of the $2\lambda_{\mathrm{s}} - \lambda_{\mathrm{s}}$ transition. In order to check this, we squeeze the coherent state on the off-phase FP and subsequently calculate the OTOC.

As a matter of fact, squeezed states in optical lattices can be achieved experimentally to an exquisite degree [40]. A squeezing protocol that is convenient for our purpose can be effectively (and unitarily) realized by reversing the time evolution, which in the experimental practice would amount to forward time propagation with reversed signs of the hopping parameter and the interaction parameter (to be done by Floquet engineering [48, 53] combined with Feshbach tuning). This means, we replace $|\xi\rangle$ by

$$|\xi(t_0)\rangle = \hat{U}(t_0)\,|\xi\rangle$$

with $t_0 = -3\tau_{\mathrm{E}}/4$, where $\hat{U}(t_0)$ is the time-evolution operator, and then calculate the OTOC, Eq. (1), for the initial state $\hat{\rho}(t_0) = |\xi(t_0)\rangle \langle \xi(t_0)|$. The corresponding

scrambling dynamics is shown in then the left panel of Fig. 7 for $N = 10^3$, while the right panel depicts the initial Husimi distribution of the squeezed state. This backward-time evaluated coherent state has a reduced linear extent along the unstable manifold. Exemplary, choosing $t_0 = -3\tau_{\mathrm{E}}/4$ (with τ_{E} the Ehrenfest time for the non-squeezed coherent state), we effectively transform $\Delta u \sim \hbar_{\mathrm{eff}}^{1/2}$ into $\Delta u \sim \hbar_{\mathrm{eff}}$. Thus, the new leaking time τ_{L}^* is now right at the Ehrenfest time, and no $2\lambda_{\mathrm{s}} - \lambda_{\mathrm{s}}$ transition is expected to exist, as fully confirmed by the numerical simulations.

IV. CONCLUSION

The OTOC associated with a wave packet that is localized around a hyperbolic fixed point in a quantum system with integrable classical (mean-field) limit under-
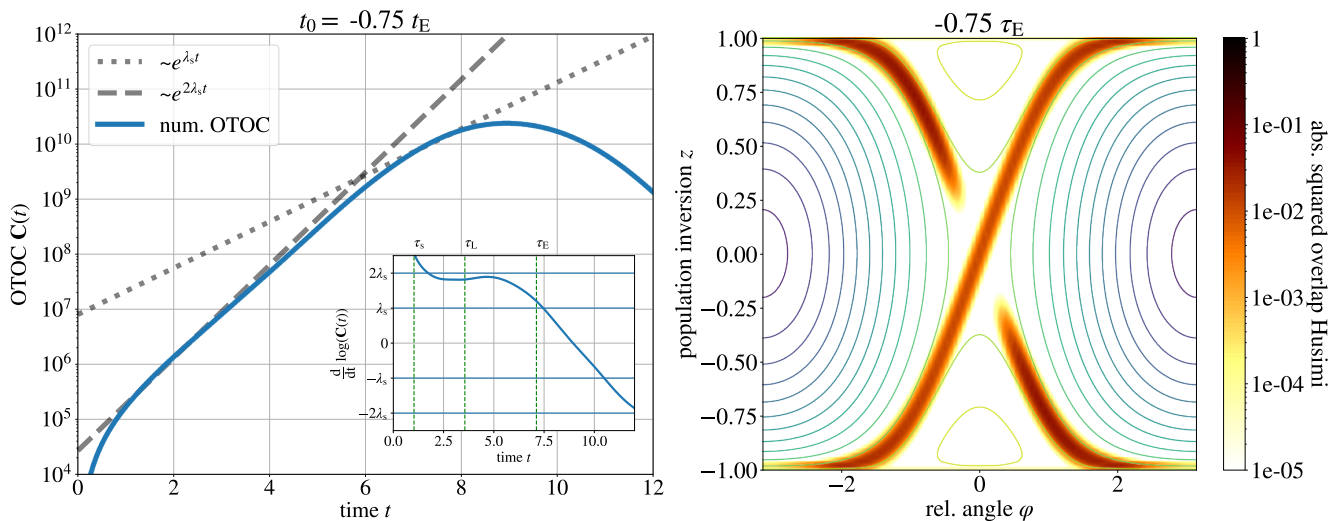
FIG. 7. Left panel: OTOC for a squeezed coherent state for the system parameter $\Theta = 1.35$ and particle number $N = 10^3$. The transition to λ_s vanishes. Right panel: Husimi distribution of the squeezed coherent state. The state is distributed along the stable manifold of the off-phase FP and features tight localization, with a width $\sim \hbar_{\text{eff}}$, along the unstable manifold.

goes a transition between different dynamical regimes, which is driven by a leaking mechanism of phase space volume along classical separatrices. If located within the pre-Ehrenfest time scale, this dynamical transition imprints a characteristic kink structure to the scrambling as measured by the exponential form of out-of-time-order correlators. Specifically, the exponential growth changes from $2\lambda_s$ to λ_s, and the kink develops for $\hbar_{\text{eff}} \to 0$, where λ_s is the stability exponent of the fixed point. We derived an analytical theory and showed how this behavior is directly related to the classical limit of the out-of-time-order correlators when their time dependence is governed by the separatrix dynamics emerging around an unstable fixed point.

Following this picture, we showed that squeezing the initial coherent state allows us to engineer the leaking time and thus the dynamical transition itself exactly as predicted by our analytical considerations.

If the phase-space localization scale of the initial state is strong enough, the leaking time is beyond the Ehrenfest time and we obtain the standard $2\lambda_s$ exponent. In contrast, an uniform state starts to leak immediately and even before the ergodic time. Therefore, the infinite temperature OTOC grows only with the reduced exponent λ_s.

We supported our picture of the dynamical transition by means of extensive simulations on the experimentally accessible, and integrable, Bose-Hubbard dimer. The extremely clean fixed point and separatrix structure of this systems allows us for a detailed study of the mechanism, and the analytical expectations of Sec. II are verified to an excellent degree.

In order to focus on separatrix effects like the leaking mechanism, requiring a very well controlled classical phase space, we restricted our numerical findings and the

corresponding analytical theory to integrable systems for which the theory in Sec. II assumes a bounded linearized regime around the fixed point. An ansatz generalizing these concepts to the realm of chaotic systems is that the role of the stability exponent λ_s from the fixed point is translated to the Lyapunov exponent λ_L from the chaotic sea, thus providing a bridge to exponential growth laws of OTOCs that were found for quantum maps with the exponents $2\lambda_L$ [54, 55] and λ_L [56], respectively. A first numerical exploration of this matter, focusing on the behaviour of OTOCs in chaotic separatrix layers, was carried out in [57], where the transition from the stability exponent λ_s associated with an unstable fixed point to the Lyapunov exponent λ_L characterizing the chaotic layer was investigated for pre-Ehrenfest time scales. In such a situation, it is an open and thrilling question to which extent the $2\lambda_s$-λ_s transition could distinguish a chaotic from an integrable system and can be generalized to mixed regular-chaotic dynamics.

V. ACKNOWLEDGMENTS

APPENDIX

A. Wigner-Moyal expansion

In this appendix we outline shortly how to obtain Eq. (2) via a Wigner-Moyal expansion. We refer for an introduction to the phase-space formalism to [52, 58, 59]. We start with the exact phase space expression for the expectation value of a general operator $\hat{O}$ given in this representation by

$$\langle \hat{O} \rangle = \text{Tr} \, \hat{\rho} \hat{O} = \iint \mathrm{d}^L q \, \mathrm{d}^L p \, W_\rho(\vec{q}, \vec{p}) O_\text{W}(\vec{q}, \vec{p})$$

where W_ρ is the Wigner function of a state described by the density operator $\hat{\rho}$, and O_W is the Wigner-Weyl symbol of the operator $\hat{O}$. Note here that O_W is a function, not an operator, i.e., $O_\text{W}(\vec{q}, \vec{p})$ is a complex number.

To proceed, we will also need the Wigner-Weyl symbol of a product of operators $\hat{A}$ and $\hat{B}$, given by the so-called star product of the corresponding Wigner-Weyl symbols as

$$\left[\hat{A}\hat{B} \right]_\text{W}(\vec{q}, \vec{p}) = A_\text{W}(\vec{q}, \vec{p}) \star B_\text{W}(\vec{q}, \vec{p})$$

where the star product is an abbreviation for

$$= A_\text{W}(\vec{q}, \vec{p}) \exp\left\{ \frac{i\hbar_\text{eff}}{2} (\overleftarrow{\nabla}_{\vec{p}} \cdot \overrightarrow{\nabla}_{\vec{q}} - \overleftarrow{\nabla}_{\vec{q}} \cdot \overrightarrow{\nabla}_{\vec{p}}) \right\} B_\text{W}(\vec{q}, \vec{p})$$

and can be expanded in $\hbar_\text{eff}$ as

$$= A_\text{W}(\vec{q}, \vec{p}) B_\text{W}(\vec{q}, \vec{p}) + \frac{i\hbar_\text{eff}}{2} \left\{ A_\text{W}(\vec{q}, \vec{p}), B_\text{W}(\vec{q}, \vec{p}) \right\} + O(\hbar_\text{eff}^2).$$

With this expression at hand, starting with Eq. (1) we easily obtain the expression

$$\mathbf{C}(t) = \iint \mathrm{d}^L q \, \mathrm{d}^L p \, W_\rho(\vec{q}, \vec{p})$$
$$\left[[\hat{A}(t), \hat{B}] \right]_\text{W}(\vec{q}, \vec{p}) \star \left[[\hat{A}(t), \hat{B}] \right]_\text{W}(\vec{q}, \vec{p}),$$

which up to this point of the manipulations is exact. Since our goal is to obtain the leading order (in the Wigner-Moyal sense) for the OTOC, the next step is to expand the two star products inside the commutator $\left[[\hat{A}(t), \hat{B}] \right]_\text{W}$ up to its first non-vanishing order

$$\left[[\hat{A}(t), \hat{B}] \right]_\text{W} = i\hbar_\text{eff} \left\{ [\hat{A}(t)]_\text{W}(\vec{q}, \vec{p}), B_\text{W}(\vec{q}, \vec{p}) \right\} + O(\hbar_\text{eff}^2).$$

As it can be derived from expanding the Heisenberg equation of motion

$$\frac{\mathrm{d}}{\mathrm{d}t} \hat{A}(t) = \frac{i}{\hbar_\text{eff}} \left[\hat{H}, \hat{A}(t) \right],$$

the time evolution of the Wigner-Weyl symbol of the operator $\hat{A}$ is given by

$$[\hat{A}(t)]_\text{W}(\vec{q}, \vec{p}) = A_\text{W}(\vec{q}(\vec{q}, \vec{p}, t), \vec{p}(\vec{q}, \vec{p}, t)) + O(\hbar_\text{eff}),$$
$$=: A_\text{W}(\vec{q}, \vec{p}, t) + O(\hbar_\text{eff}),$$

where $\vec{q}(\vec{q}, \vec{p}, t)$ and $\vec{p}(\vec{q}, \vec{p}, t)$ are the classical evolved phase space points. One then can verify that the in leading order the quantum and classical equations of motion agree since the quantum commutator reduces to the classical Poisson-bracket. Putting all together, we arrive to the leading order result we in Eq. (2)

$$\mathbf{C}(t) = \hbar_\text{eff}^2 \langle W_\rho(\vec{q}_0, \vec{p}_0) \left| \left\{ A_\text{W}(\vec{q}_0, \vec{p}_0, t), B_\text{W}(\vec{q}_0, \vec{p}_0) \right\} \right|^2 \rangle_\text{PS} + O(\hbar_\text{eff}^3),$$

where we suppressed the phase-space integral into $\langle . \rangle_\text{PS}$ and renamed $(\vec{q}, \vec{p})$ to $(\vec{q}_0, \vec{p}_0)$.

[1] Q. Hummel, B. Geiger, J. D. Urbina, and K. Richter, Phys. Rev. Lett. **123**, 160401 (2019).
[2] T. Xu, T. Scaffidi, and X. Cao, Phys. Rev. Lett. **124**, 140602 (2020).
[3] S. Xu and B. Swingle, (2022), arXiv:2202.07060 [quant-ph].
[4] K. Richter, J. D. Urbina, and S. Tomsovic, Journal of Physics A: Mathematical and Theoretical **55**, 453001 (2022).
[5] J. Maldacena, S. H. Shenker, and D. Stanford, Journal of High Energy Physics **2016** (2016).
[6] P. Hayden and J. Preskill, Journal of High Energy Physics **2007**, 120 (2007).
[7] Y. Sekino and L. Susskind, Journal of High Energy Physics **2008**, 065 (2008).
[8] Y. Gu and A. Kitaev, Journal of High Energy Physics **2019** (2019), 10.1007/jhep02(2019)075.

[9] B. Kobrin, Z. Yang, G. D. Kahanamoku-Meyer, C. T. Olund, J. E. Moore, D. Stanford, and N. Y. Yao, Phys. Rev. Lett. **126**, 030602 (2021).
[10] N. Tsuji and P. Werner, Phys. Rev. B **99**, 115132 (2019).
[11] A. I. Larkin and Y. N. Ovchinnikov, Soviet Journal of Experimental and Theoretical Physics **28**, 1200 (1969).
[12] B. Swingle, G. Bentsen, M. Schleier-Smith, and P. Hayden, Phys. Rev. A **94**, 040302 (2016).
[13] M. Gärttner, J. G. Bohnet, A. Safavi-Naini, M. L. Wall, J. J. Bollinger, and A. M. Rey, Nature Physics **13**, 781 (2017).
[14] J. Li, R. Fan, H. Wang, B. Ye, B. Zeng, H. Zhai, X. Peng, and J. Du, Phys. Rev. X **7**, 031011 (2017).
[15] R. A. Kidd, A. Safavi-Naini, and J. F. Corney, Phys. Rev. A **102**, 023330 (2020).
[16] H. Shen, P. Zhang, R. Fan, and H. Zhai, Phys. Rev. B **96**, 054503 (2017).

[17] A. Bohrdt, C. B. Mendl, M. Endres, and M. Knap, New Journal of Physics **19**, 063001 (2017).

[18] J. Rammensee, J. U. Urbina, and K. Richter, Phys. Rev. Lett. **121**, 124101 (2018).

[19] S. Pappalardi, A. Russomanno, B. Žunkovič, F. Iemini, A. Silva, and R. Fazio, Phys. Rev. B **98**, 134303 (2018).

[20] B. Geiger, J. D. Urbina, and K. Richter, Phys. Rev. Lett. **126**, 110602 (2021).

[21] D. Villaseñor, S. Pilatowsky-Cameo, M. A. Bastarrachea-Magnani, S. Lerma-Hernández, L. F. Santos, and J. G. Hirsch, Entropy **25** (2023), 10.3390/e25010008.

[22] L. Benet, F. Borgonovi, F. M. Izrailev, and L. F. Santos, (2022), arXiv:2211.10451 [cond-mat.stat-mech].

[23] S. Pilatowsky-Cameo, J. Chávez-Carlos, M. A. Bastarrachea-Magnani, P. Stránský, S. Lerma-Hernández, L. F. Santos, and J. G. Hirsch, Phys. Rev. E **101**, 010202 (2020).

[24] R. A. Kidd, A. Safavi-Naini, and J. F. Corney, Phys. Rev. A **103**, 033304 (2021).

[25] K. Hashimoto, K.-B. Huh, K.-Y. Kim, and R. Watanabe, Journal of High Energy Physics **2020** (2020), 10.1007/jhep11(2020)068.

[26] I. García-Mata, M. Saraceno, R. A. Jalabert, A. J. Roncaglia, and D. A. Wisniacki, Phys. Rev. Lett. **121**, 210601 (2018).

[27] E. Fortes, I. Garcia-Mata, R. Jalabert, and D. Wisniacki, Physical Review E **100** (2019), 10.1103/PhysRevE.100.042201.

[28] A. Polkovnikov, K. Sengupta, A. Silva, and M. Vengalattore, Rev. Mod. Phys. **83**, 863 (2011).

[29] W. P. Schleich, *Quantum Optics in Phase Space* (Wiley-VCH, Berlin, 2001).

[30] Y. S. Kim and M. E. Noz, *Phase Space Picture of Quantum Mechanics* (World Scientific, 1991).

[31] R. F. O'Connell, International Journal of Quantum Information **06**, 415 (2008).

[32] M. Gutzwiller, *Chaos in Classical and Quantum Mechanics*, Interdisciplinary Applied Mathematics (Springer New York, 1991).

[33] F. Haake, *Quantum Signatures of Chaos*, Physics and astronomy online library (Springer, 2001).

[34] M. Brack and R. Bhaduri, *Semiclassical Physics*, Frontiers in physics (Avalon Publishing, 1997).

[35] M. Akila, D. Waltner, B. Gutkin, P. Braun, and T. Guhr, Phys. Rev. Lett. **118**, 164101 (2017).

[36] P. Braun, D. Waltner, M. Akila, B. Gutkin, and T. Guhr, Phys. Rev. E **101**, 052201 (2020).

[37] T. Engl, J. D. Urbina, and K. Richter, Phys. Rev. E **92**, 062907 (2015).

[38] M. Tabor, *Chaos and Integrability in Nonlinear Dynamics: An Introduction* (Wiley, 1989).

[39] S. Wiggins, *Introduction to Applied Nonlinear Dynamical Systems and Chaos*, Texts in Applied Mathematics (Springer New York, 2003).

[40] J. Estève, C. Gross, A. Weller, S. Giovanazzi, and M. K. Oberthaler, Nature **455**, 1216 (2008).

[41] R. A. Jalabert, I. García-Mata, and D. A. Wisniacki, Phys. Rev. E **98**, 062218 (2018).

[42] B. Geiger, *From few to many particles: Semiclassical approaches to interacting quantum systems*, Vol. 55 (University of Regensburg, 2020).

[43] E. Il'ichev, M. Grajcar, R. Hlubina, R. P. J. IJsselsteijn, H. E. Hoenig, H.-G. Meyer, A. Golubov, M. H. S. Amin, A. M. Zagoskin, A. N. Omelyanchouk, and M. Y. Kupriyanov, Phys. Rev. Lett. **86**, 5369 (2001).

[44] M. Albiez, R. Gati, J. Fölling, S. Hunsmann, M. Cristiani, and M. K. Oberthaler, Phys. Rev. Lett. **95**, 010402 (2005).

[45] S. Fölling, S. Trotzky, P. Cheinet, M. Feld, R. Saers, A. Widera, T. Müller, and I. Bloch, Nature **448**, 1029 (2007).

[46] D. Witthaut, F. Trimborn, and S. Wimberger, Phys. Rev. Lett. **101**, 200402 (2008).

[47] P. Cheinet, S. Trotzky, M. Feld, U. Schnorrberger, M. Moreno-Cardoner, S. Fölling, and I. Bloch, Phys. Rev. Lett. **101**, 090404 (2008).

[48] E. Kierig, U. Schnorrberger, A. Schietinger, J. Tomkovic, and M. K. Oberthaler, Phys. Rev. Lett. **100**, 190405 (2008).

[49] J. Tomkovič, W. Muessel, H. Strobel, S. Löck, P. Schlagheck, R. Ketzmerick, and M. K. Oberthaler, Phys. Rev. A **95**, 011602 (2017).

[50] J. Negele and H. Orland, *Quantum Many Particle Systems* (Basic Books, 1995).

[51] D. K. Campbell, in *Strongly Coupled Field Theories for Condensed Matter and Quantum Information Theory*, edited by A. Ferraz, K. S. Gupta, G. W. Semenoff, and P. Sodano (Springer International Publishing, Cham, 2020) pp. 247–258.

[52] C. Gardiner, P. Zoller, and P. Zoller, *Quantum Noise: A Handbook of Markovian and Non-Markovian Quantum Stochastic Methods with Applications to Quantum Optics*, Springer Series in Synergetics (Springer, 2004).

[53] H. Lignier, C. Sias, D. Ciampini, Y. Singh, A. Zenesini, O. Morsch, and E. Arimondo, Phys. Rev. Lett. **99**, 220403 (2007).

[54] E. B. Rozenbaum, S. Ganeshan, and V. Galitski, Physical Review Letters **118** (2017), 10.1103/physrevlett.118.086801.

[55] I. García-Mata, M. Saraceno, R. A. Jalabert, A. J. Roncaglia, and D. A. Wisniacki, Phys. Rev. Lett. **121**, 210601 (2018).

[56] A. Lakshminarayan, Phys. Rev. E **99**, 012201 (2019).

[57] F. Meier, M. Steinhuber, J. D. Urbina, D. Waltner, and T. Guhr, Phys. Rev. E **107**, 054202 (2023).

[58] W. B. Case, American Journal of Physics **76**, 937 (2008).

[59] T. L. Curtright and C. K. Zachos, Asia Pacific Physics Newsletter **01**, 37 (2012).